Contour Advection with Surgery: A Technique for Investigating Finescale Structure in Tracer Transport

DARRYN W. WAUGH AND R. ALAN PLUMB

Center for Meteorology and Physical Oceanography, Massachusetts Institute of Technology, Cambridge, Massachusetts

(Manuscript received 28 October 1992, in final form 10 May 1993)

ABSTRACT

We present a trajectory technique, contour advection with surgery (CAS), for tracing the evolution of material contours in a specified (including observed) evolving flow. CAS uses the algorithms developed by Dritschel for contour dynamics/surgery to trace the evolution of specified contours. The contours are represented by a series of particles, which are advected by a specified, gridded, wind distribution. The resolution of the contours is preserved by continually adjusting the number of particles, and finescale features are produced that are not present in the input data (and cannot easily be generated using standard trajectory techniques). The reliability, and dependence on the spatial and temporal resolution of the wind field, of the CAS procedure is examined by comparisons with high-resolution numerical data (from contour dynamics calculations and from a general circulation model), and with routine stratospheric analyses. These comparisons show that the large-scale motions dominate the deformation field and that CAS can accurately reproduce small scales from low-resolution wind fields. The CAS technique therefore enables examination of atmospheric tracer transport at previously unattainable resolution.

1. Introduction

High-resolution, idealized simulations of the stratospheric polar vortex (e.g., Juckes and McIntyre 1987; Juckes 1989; Salby et al. 1990; Waugh 1993; Norton 1994) illustrate that much of the transport of potential vorticity and material tracers is associated with the production of thin filamentary structures and that the vortex has a very sharp edge. Such finescale features are clearly evident, for example, in aircraft observations of chemical tracers in the lower stratosphere (Anderson et al. 1989; Murphy et al. 1992; Tuck et al. 1992). However, a major difficulty in the interpretation of these localized in situ measurements in terms of the large-scale flow is the lack of comparable resolution in the meteorological analyses. Without being able to put such measurements into the large-scale context, we are limited in our ability to quantify or, in the absence of localized, high-resolution in situ data, even to detect the transport of material across the vortex edge. Moreover, without information about the behavior at scales smaller than those of the analyses we are unable to test the prediction of most high-resolution models that the vortex is isolated from intrusions of midlatitude air.

Analyses of material motions in a given flow are traditionally based on calculations of trajectories of material particles in that flow. Attempts to examine finescale features in these flows using standard trajectory techniques frequently fail because the generation of finescales cannot be resolved unless new trace particles are continually generated (e.g., see Fig. 11). One approach (e.g., Pierce and Fairlie 1993) is to begin with a sufficiently large number of particles to maintain adequate resolution through the period of interest. Another is to add new particles as required to resolve developing small-scale features. Schoeberl and Bacmeister (1993) used a scheme in which new particles are added when the distance between existing particles exceeds a critical value. In this paper we describe a sophisticated contour–trajectory technique, which we refer to as contour advection with surgery (CAS), in which the number and placement of particles along a contour is continually adjusted, using the algorithms developed by Dritschel (1988, 1989) for contour dynamics/surgery (CDS). Nôrton (1994) has independently used the same particle redistribution algorithm to investigate the finescale evolution of material contours in a shallow-water model of a disturbed polar vortex.

The CAS technique can reproduce the finescale structure of material contours in a known flow of relatively modest spatial and temporal resolution. The evolution of a specified material contour is traced by representing the contour by a series of particles and advecting these particles by the wind interpolated (in space and time) from the specified, gridded distribution. The resolution of the contours is preserved by automatically (and efficiently) adjusting the number of particles, and enables generation of small-scale features. At the same time the number of particles is main-

Corresponding author address: Dr. R. Alan Plumb, Center for Meteorology and Physical Oceanography, Massachusetts Institute of Technology, Room 54-1726, Cambridge, MA 02139.

tained at a computationally manageable level by including a "surgery" procedure that disconnects and reconnects contours where and when appropriate. The contour representation and surgery is the same as in CDS and is outlined in the next section.

Preliminary investigations using CAS for diagnosing stratospheric air motions during participation in the National Aeronautics and Space Administration's second Airborne Arctic Stratosphere Experiment were encouraging and suggest that the CAS technique is more effective for tracer transport studies than conventional methods. However, it is not obvious how accurately the small scales can be predicted by advecting material contours with a low-resolution (in space and time) representation of the actual wind. The usefulness of the results will depend on the extent to which the deformation field is dominated by the large-scale motions. In this paper we test the reliability of the CAS procedure under various conditions and, in particular, demonstrate the insensitivity of the CAS results to the spatial and temporal resolution of the wind field. Comparisons of CAS calculations with aircraft observations of chemical tracers are discussed elsewhere (Plumb et al. 1994; Waugh et al. 1994).

The outline of this paper is as follows. In the next section the basic CAS algorithm is described. Then in section 3 the accuracy of the method is investigated by comparisons of CAS calculations, using wind fields of varying resolution, with a CDS calculation of a forced polar vortex (Waugh 1993). The reliability is further tested by performing CAS calculations using data from the high-resolution Geophysical Fluid Dynamics Laboratory "SKYHI" general circulation model (section 4) and stratospheric analyses of the National Meteorological Center (NMC) (section 5). These comparisons show that the large-scale motions dominate the deformation field and that CAS can, in most circumstances, accurately reproduce the generation of small scales from low-resolution wind fields and produce features that are not present in the low-resolution input data.

2. Basic algorithm

The input for CAS calculations consists of the initial distribution of a materially conserved quantity (represented by N contours) and the wind field stored on a latitude–longitude grid ($\Delta\phi$ by $\Delta\lambda$) at time interval ΔT. Each contour is represented by a series of material particles, and the evolution of the contour is then determined by advecting each particle by the velocity (calculated by spatial and temporal interpolation from the gridded data) at that particle (a time step much smaller than ΔT is used in the advection scheme). As a flow evolves, small scales generally develop and it becomes necessary to add particles in order to maintain accurate resolution of the contours. This means that, if a flow continually develops small scales, the number of particles continually increases; therefore, to keep the calculations computationally manageable, a truncation, or "surgery," of small scales is performed.

In the present CAS scheme, linear interpolation is used to determine the velocity at each particle and the particles are advected using a fourth-order Runge–Kutta scheme (with a one-hour time step). The contour representation is the same as in the CDS algorithm of Dritschel (1988, 1989); full details of the contour representation and surgery procedure are given in these references, and only a brief description is included here. Each contour is represented using cubic spline interpolation between particles, and the number and placement of the particles depends on a prescribed dimensionless parameter μ (approximately $2\pi/\mu$ particles are used to represent a contour around a latitude circle) and the curvature of the contour (the number of particles per unit length is approximately proportional to the two-thirds power of the curvature). Note that particle redistribution schemes that use only the distance between adjacent particles may not capture some small-scale features [see Dritschel (1989) and references therein]. The algorithm automatically removes features below some prescribed surgery, or cutoff, scale δ. If two identical contours (or two different sections of the same contour) are within this surgery scale, the contours are joined. This surgery means that excessively thin filaments are shortened, and it also enables two contours to merge into one (or conversely, a single contour to break into two). It is important to note that this surgery only effects small-scale filamentary structures and does not prevent the formation of arbitrarily steep material gradients.

The accuracy of CAS calculations depends on the quality of the input data, the interpolation used to calculate the velocity from the gridded data, and the contour representation and surgery. The accuracy of the contour representation and surgery has been investigated in detail (Dritschel 1988, 1989), and we concentrate here on the effect of the resolution of the input data on the accuracy of CAS calculations. In all calculations in this paper we use linear interpolation to calculate the velocity from the grid and use parameter values $\mu = 0.10$ and $\delta = \mu^2 R/8$. (For a sphere of radius $R = 6371$ km, this corresponds to a surgery scale $\delta \approx 8$ km.) To determine how the accuracy of CAS calculations depends on the input data, we have performed many calculations with velocity grids of various spatial ($\Delta\phi$, $\Delta\lambda$) and temporal (ΔT) resolution and also with differing resolution of initial material contours.

3. Comparisons with a CDS calculation

In this section we investigate the accuracy of CAS calculations by performing a series of calculations tracing the evolution of potential vorticity (PV) contours using velocity data of different spatial and temporal resolution generated from a CDS calculation and com-

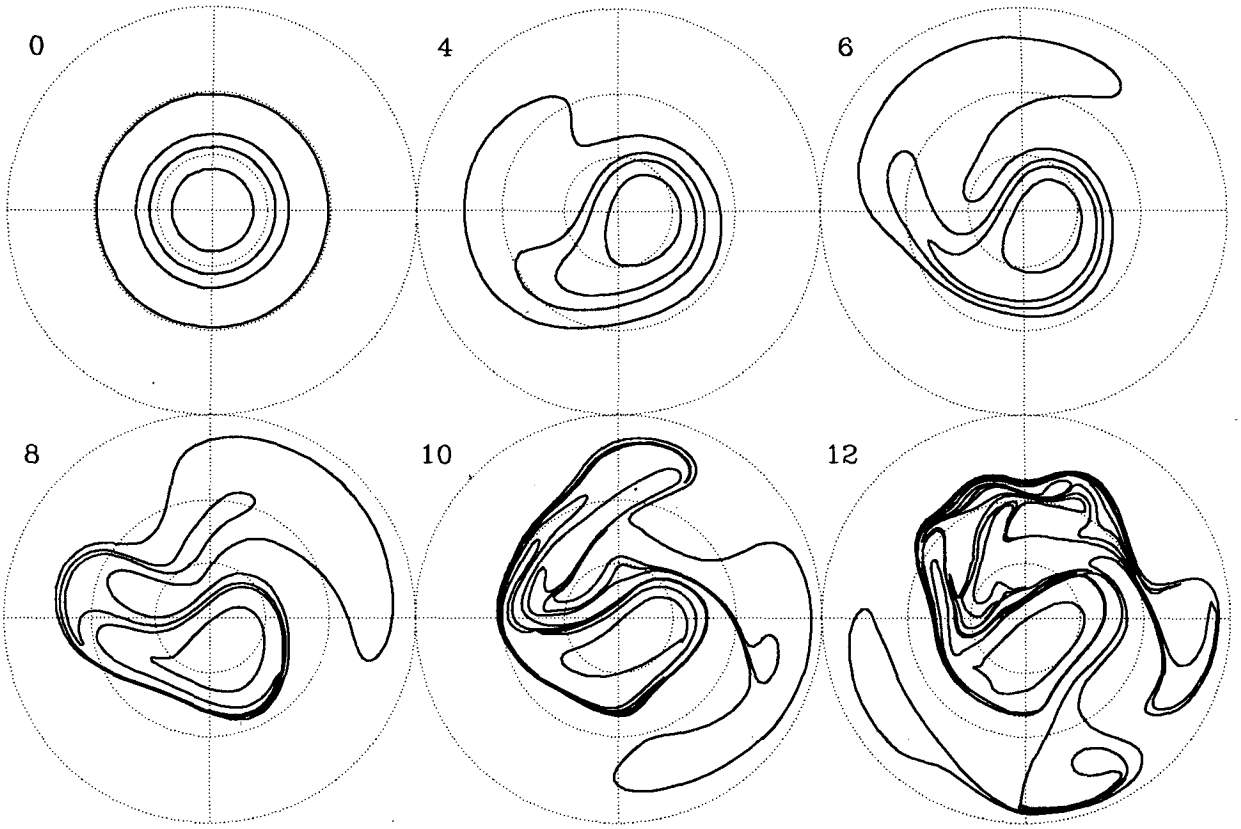

FIG. 1. Hemispherical CDS calculation of a polar vortex disturbed by zonal wavenumber 1 topographic forcing. The initial potential vorticity distribution is represented by $N = 21$ contours, and the forcing is slowly turned on over the first 4 days. See Waugh (1993) for full details. Only the four contours used in the CAS calculations are shown in the plots. Plots are polar stereographic projections; latitudinal circles at 0°, 30°N, and 60°N are marked, and 0° longitude is at the bottom of each plot. Time (in days) is to the upper left of each plot.

paring the results with the original CDS calculation. Using a CDS calculation as a test flow has the advantage that the only difference between CDS and CAS calculations is the way in which the velocity at each particle is determined. In CDS calculations the velocity at each particle is determined instantaneously, accurately, and locally, via contour integrals around the contours of PV discontinuity, whereas in CAS calculations the velocity at each particle is determined by spatial and temporal interpolation from a grid (the velocity at each point on the grid is determined by the same contour integrals as in CDS calculations). Therefore, within the accuracy of the contour representation, which is the same in both calculations, the differences between CDS and CAS calculations are due only to errors caused by the spatial and temporal interpolation of the velocity from the grid and not due to errors in the velocity at each grid point.

The CDS calculation used in the comparison is a (21 contour) barotropic calculation of a polar vortex disturbed by zonal harmonic wave 1 topographic forcing discussed in Waugh (1993). This calculation is representative of a disturbed stratospheric polar vortex; that is, there is Rossby wave breaking with tongues of PV drawn out of the vortex and mixed into the surrounding surf zone. Although the CDS calculation used 21 contours we consider only 4 contours in the CAS calculations. Figure 1 shows the evolution of these four contours in the full CDS calculation [see Fig. 2 of Waugh (1993) for evolution of all 21 contours].

The output from a CAS calculation with $\Delta\phi \times \Delta\lambda = 2° \times 5°$ and $\Delta T = 12$ h is shown in Fig. 2. Comparing with Fig. 1 we see that the evolution of the contours in the CAS calculation is very similar to that in the CDS calculation, with the only noticeable differences being the structure at the end of filaments. (The CAS calculation is not quite reproducing the same "roll up" of the filament tips as in the exact CDS flow.) These differences are, however, small, and the overall agreement between the calculations is excellent, even for finescale structures.

The sensitivity of the CAS calculation to the spatial resolution of the advecting velocity field is shown in Fig. 3, which shows the position of the contours at day 12 for CAS calculations with $\Delta\phi \times \Delta\lambda$ equal to (a) $5° \times 10°$ and (b) $1° \times 3°$. Comparing these plots (and

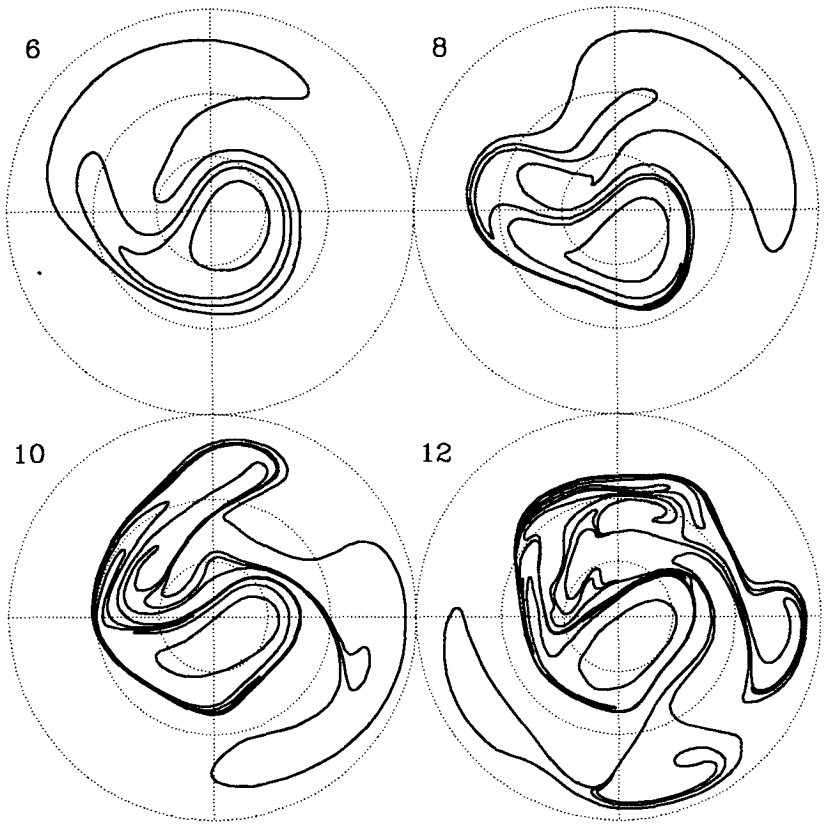

FIG. 2. Output from a CAS calculation of the flow shown in Fig. 1. The spatial resolution of the advecting velocity field is $\Delta\phi \times \Delta\lambda = 2° \times 5°$, and the grid is stored at $\Delta T = 12$ h.

Figs. 1 and 2) we see that there are only very small differences between CAS calculations using different grid resolutions, suggesting that a $5° \times 10°$ grid is sufficient for the CAS calculations and that there is little advantage of going to a higher-resolution grid (at least when there are no errors in the velocity at each grid point). This relative insensitivity to the spatial resolution of the velocity grid implies that the large-scale motions dominate the deformation field in this flow.

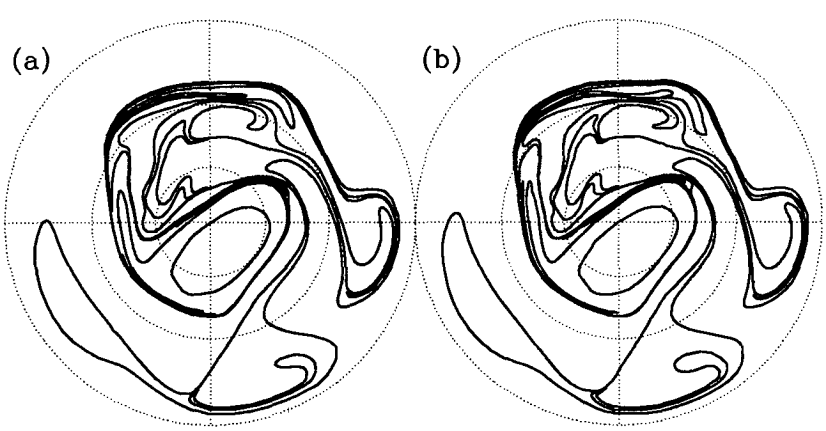

FIG. 3. Potential vorticity contours at day 12 from CAS calculations using an advecting velocity field with $\Delta\phi \times \Delta\lambda$ equal to (a) $5° \times 10°$, and (b) $1° \times 3°$; $\Delta T = 12$ h in both calculations.

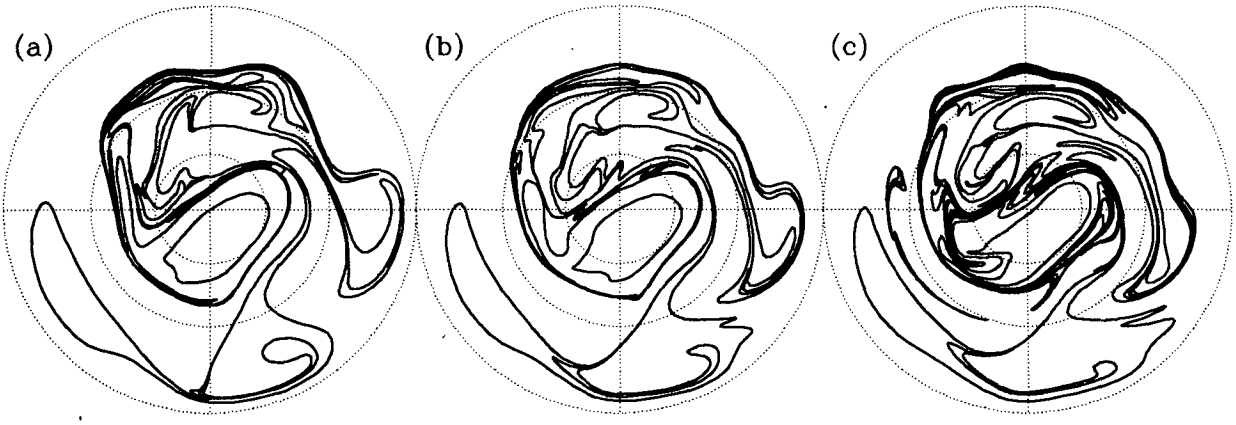

FIG. 4. As in Fig. 3 but with $\Delta\phi \times \Delta\lambda = 2° \times 5°$ and ΔT equal to (a) 6 h, (b) 18 h, and (c) 24 h.

Figure 4 shows the dependence of the CAS calculation on the temporal resolution of the velocity grid. From these plots we see that CAS calculations are much more sensitive to temporal than to spatial resolution. When the time interval ΔT is decreased to 6 h (Fig. 4a) there is a marked improvement in the structure of the ends of filaments (i.e., the roll-up of the filaments is much closer to that in the exact flow). On the other hand, if ΔT is increased to 18 h or more, large differences start to appear between the CAS and CDS calculations (Figs. 4b,c). The structure of some of the filaments is quite different, and spurious small scales develop in the CAS calculation. It therefore appears that for this flow ΔT must be less than 1 day for reasonably accurate CAS calculations, although as shown later the maximum ΔT for accurate calculations is sensitive to the characteristics of the flow being considered.

The preceding comparisons have considered CAS calculations with the exact initial PV distribution. What is the effect of the initial PV not being accurately resolved? To investigate the effect of the initial distribution, CAS calculations have been performed using initial distributions of varying resolution and starting at different times (e.g., using the initial PV field as that calculated from the $5° \times 10°$ velocity grid at $t = 8$). These calculations show that although features missing from poorly resolved initial conditions will lead to features missing from the subsequent evolution, the generation of new structures is relatively little affected by the initial resolution.

The calculations in this section have shown that accurate CAS calculations can be performed using space/time resolution available in routine global analyses and that the small-scale features thus produced are remarkably similar to those in the exact flow. The accuracy, and advantage, of the CAS calculations is even more apparent if the results are compared with the low-resolution PV field corresponding to the gridded velocity data. Figure 5 shows the PV at day 12 calculated (using a finite-difference scheme) from the (a) $5° \times 10°$, (b) $2° \times 5°$, and (c) $1° \times 3°$ velocity grids. These fields

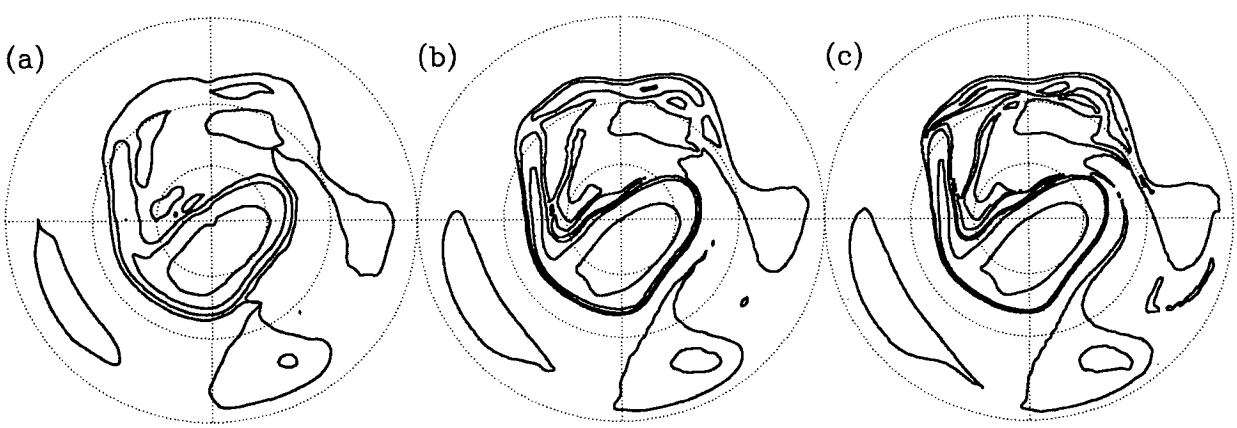

FIG. 5. Potential vorticity contours, at day 12, calculated (using a finite-difference scheme) from the velocity grid with $\Delta\phi \times \Delta\lambda$ equal to (a) $5° \times 10°$, (b) $2° \times 5°$, and (c) $1° \times 3°$.

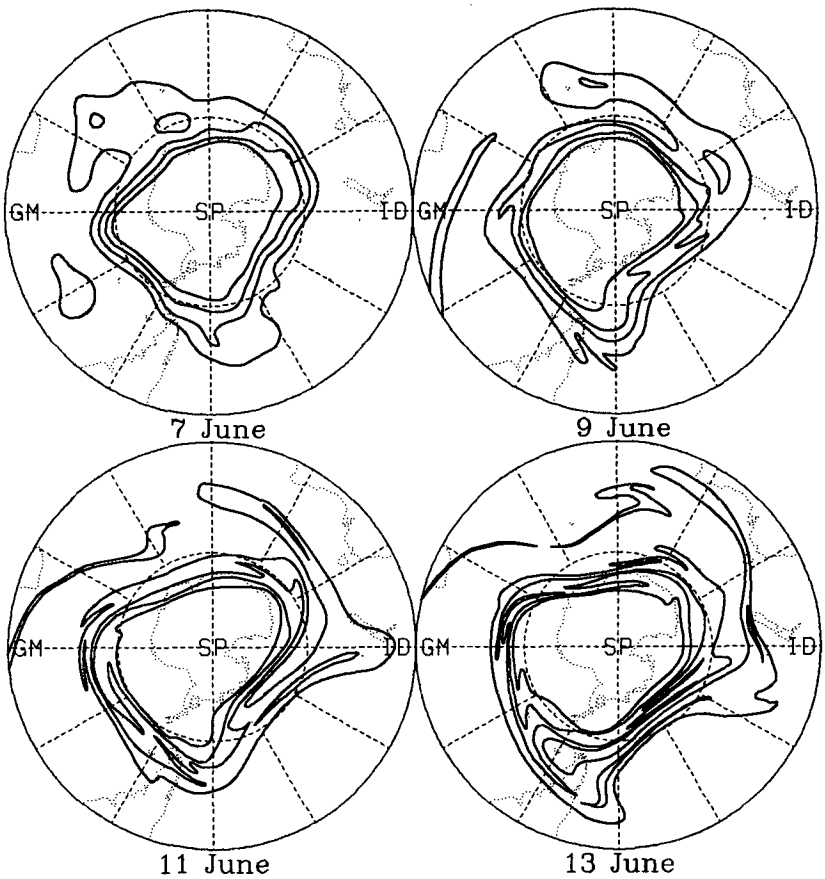

FIG. 6. Output from a 6-day CAS calculation using SKYHI data. At the start of the calculation the contours correspond to PV contours $Q = (-1.8, -2.0, -2.2, -2.4) \times 10^{-5}$ K m^2 g^{-1} s^{-1} on the 450 K isentropic surface at 0300 UTC 7 June. The advecting velocity field has spatial resolution $\Delta\phi \times \Delta\lambda = 1° \times 1.2°$, and temporal resolution $\Delta T = 12$ h. Plots are polar stereographic projections; latitudinal circles 30°S (solid) and 60°S (dashed) are marked.

contain only large-scale structures (with the exception of the PV from the 1° × 3° grid, which contains a few filamentary structures). The CAS calculations can successfully generate small-scale filaments, albeit with some inaccuracies in detail, that are not present at all in the PV formed from the low-resolution input data.

4. CAS calculations using SKYHI GCM data

We now use data from a more realistic flow to test the accuracy of CAS calculations. The data are 3-h winds from the high-resolution GFDL 'SKYHI' GCM (Mahlman and Umscheid 1987), which has horizontal resolution of 1° lat by 1.2° long. CAS calculations of the evolution of the Southern Hemisphere PV on the 450 K isentropic surface have been performed, using velocity grids of varying spatial and temporal resolution.

Unfortunately, there is a large amount of incoherent small-scale structure in the PV fields generated from the SKYHI data. A detailed comparison therefore has not been made between CAS calculations and the SKYHI data, and all comparisons in this section will be between CAS calculations using velocity grids with different resolution. All CAS calculations use an initial PV distribution that is truncated to 29 spherical harmonics (T29) and thus does not contain small-scale features.

Figure 6 shows the output from a 6-day CAS calculation from 7 June using the full spatial resolution, but temporal resolution $\Delta T = 12$ h. During this period there is a wave breaking event with material being ejected from the vortex. Note, however, that the vortex is not as active as in the CDS calculation in Fig. 1, and only a small amount of material is ejected during the wave breaking. Also note that during this period low PV air is wrapped around the polar vortex (e.g., at 50°S, 60°W on 13 June)—a feature that can also be observed in the SKYHI PV data.

Two series of experiments were run to test the sensitivity of these results to different spatial resolution (Fig. 7) and temporal resolution (Fig. 8) of the input

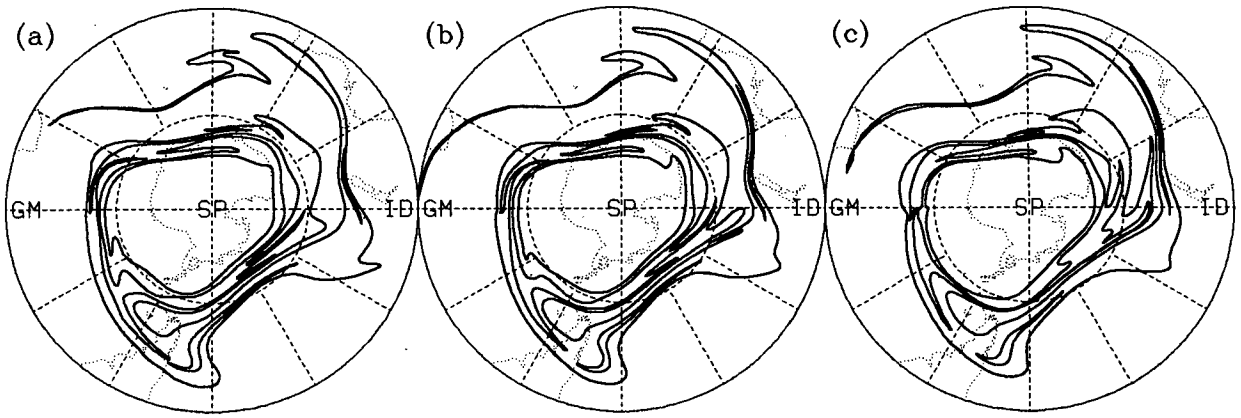

FIG. 7. Potential vorticity contours at 0300 UTC 13 June for CAS calculation with $\Delta\phi \times \Delta\lambda$ = (a) 3° × 3.6°, (b) 5° × 6°, and (c) 10° × 12° (ΔT = 12 h).

winds. The calculations using grids of different spatial resolution (compare Figs. 6 and 7) show that the results are relatively insensitive to the spatial resolution and that small scales can be accurately reproduced using a wind field on a grid as coarse as 10° × 12°. Calculations with different temporal resolution (compare Figs. 6 and 8), however, show that reasonably accurate calculations can in this case be performed using daily wind fields and that significant differences develop only when ΔT is greater than 1 day. It therefore seems that the necessary temporal resolution for accurate calculations depends on the characteristics of the flow. For a flow involving vigorous wave breaking (e.g., Fig. 1) a smaller ΔT will be required than in a flow that is less active (e.g., Fig. 6).

5. CAS calculations using NMC stratospheric analyses

We have performed several CAS calculations using NMC stratospheric analyses for Northern Hemisphere winter 1991/92. The contours were initially specified to coincide with the analyzed positions of PV contours on the 450 K isentropic surface and were advected by the NMC analyzed winds on the 450 K surface (resolution 2° lat × 5° long, once per day). Comparisons of the CAS calculation with the analyzed location of the PV contours are very encouraging; an example is shown in Figs. 9 and 10.

This CAS calculation was run as a test of the interpretation of the analyzed PV field (Fig. 9) as indicating an intrusion of midlatitude air into the vortex. The initial distribution of contours on 16 January shows a predominantly triangular-shaped vortex. Six days later, the CAS calculation shows a kidney-shaped vortex (the edge of the vortex is marked by the closeness of the contours) with an intrusion of midlatitude air into the vortex (e.g., 60°N, 45°E); see Fig. 10a. This PV distribution does indeed appear remarkably consistent with the 22 January analyzed PV and, specifically, confirms the reality of the intrusion event. Direct observational evidence for the reality of this event, and the

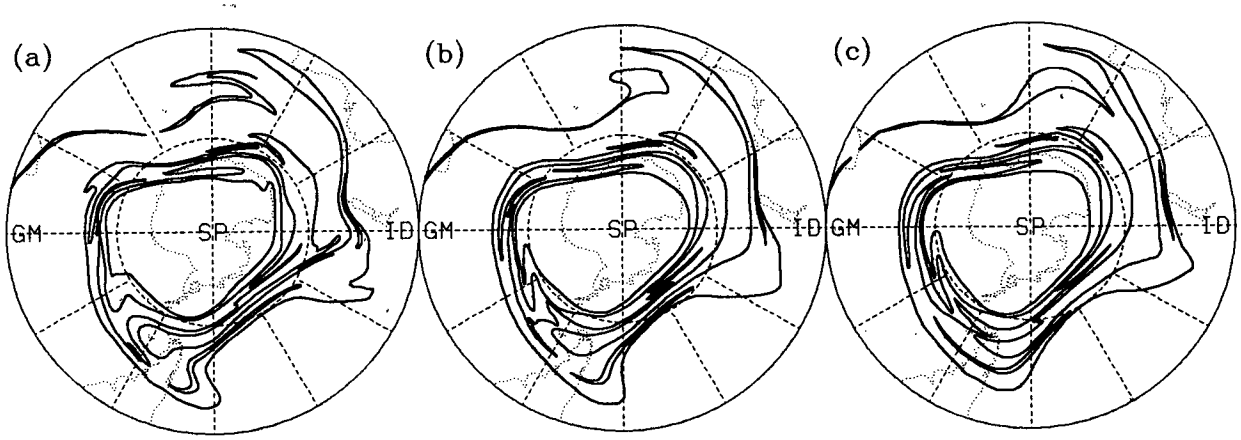

FIG. 8. As in Fig. 7 but with ΔT = (a) 6 h, (b) 24 h, and (c) 48 h ($\Delta\phi \times \Delta\lambda$ = 1° × 1.2°).

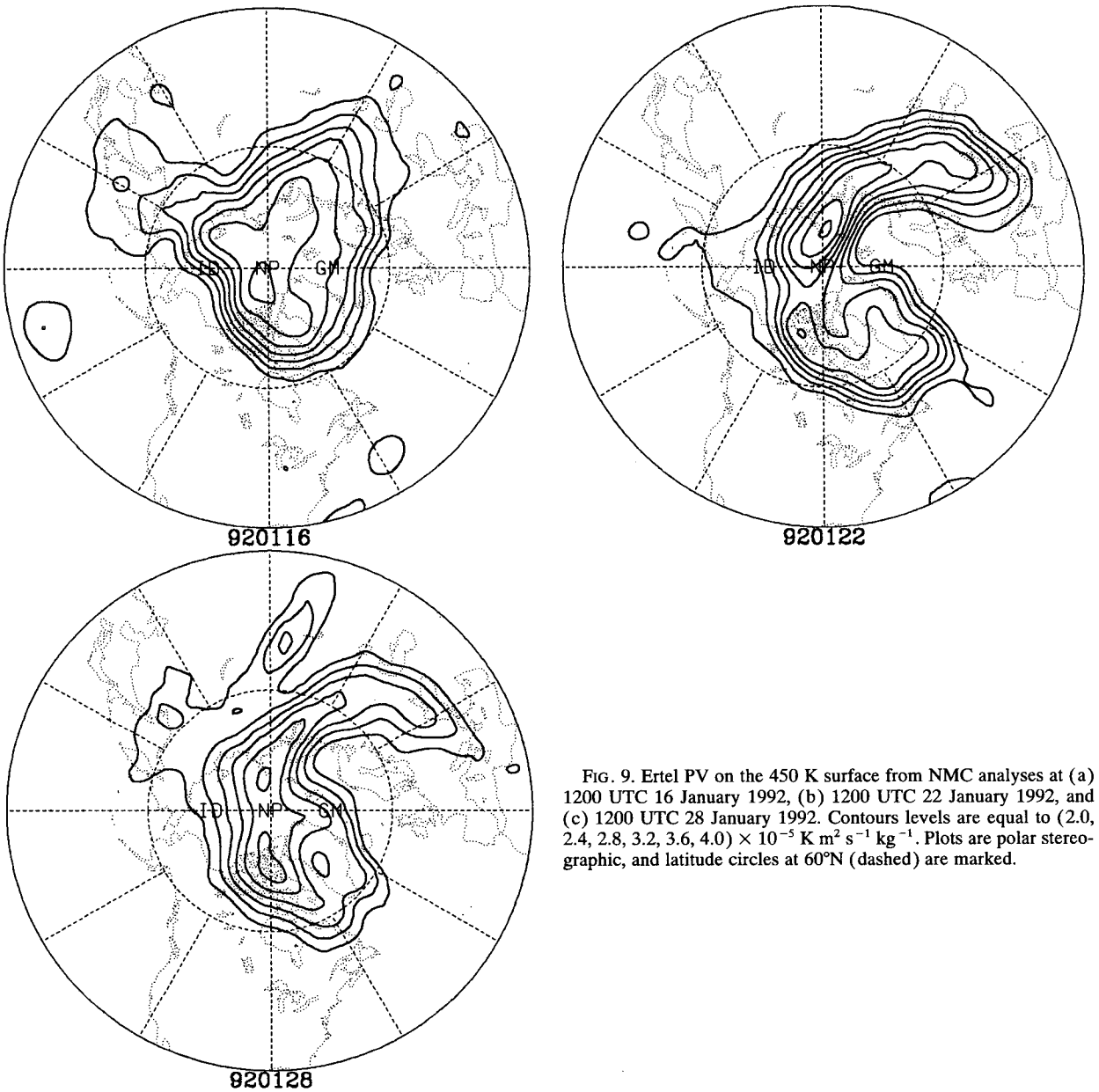

FIG. 9. Ertel PV on the 450 K surface from NMC analyses at (a) 1200 UTC 16 January 1992, (b) 1200 UTC 22 January 1992, and (c) 1200 UTC 28 January 1992. Contours levels are equal to (2.0, 2.4, 2.8, 3.2, 3.6, 4.0) $\times 10^{-5}$ K m^2 s^{-1} kg^{-1}. Plots are polar stereographic, and latitude circles at 60°N (dashed) are marked.

accuracy of the CAS results, is presented in Plumb et al. (1994). The CAS calculation has been continued for another six days, and there is still a remarkable agreement between the CAS contours (Fig. 10b) and the analyzed PV (Fig. 9c). In particular, both maps show outbreaks of high PV air into midlatitudes—for example, at 45°W, 80°W, and 150°W. Note that the CAS calculation produces a vortex with a very sharp vortex edge, and there is stirring and finescale structure both outside and inside the vortex. These finescale features captured in CAS computations cannot generally be confirmed by the low-resolution analyses. However, comparisons with chemical observations made during NASA's Airborne Arctic Stratosphere Experiments has confirmed the reality of the filamentary structures in CAS calculations (Waugh et al. 1994).

As mentioned in the Introduction, finescale structures cannot be easily predicted using standard trajectory techniques in which the number of material particles is fixed. As an example, Fig. 11 compares the evolution of the 3.2 $\times 10^{-5}$ K m^2 s^{-1} kg^{-1} contour of Ertel PV, for the period shown in Fig. 9, using (a) a standard trajectory code with 68 particles and (b) the CAS code. Although the calculation using the standard method indicates an intrusion on 22 January, it does not resolve the shape as well as CAS. As the standard

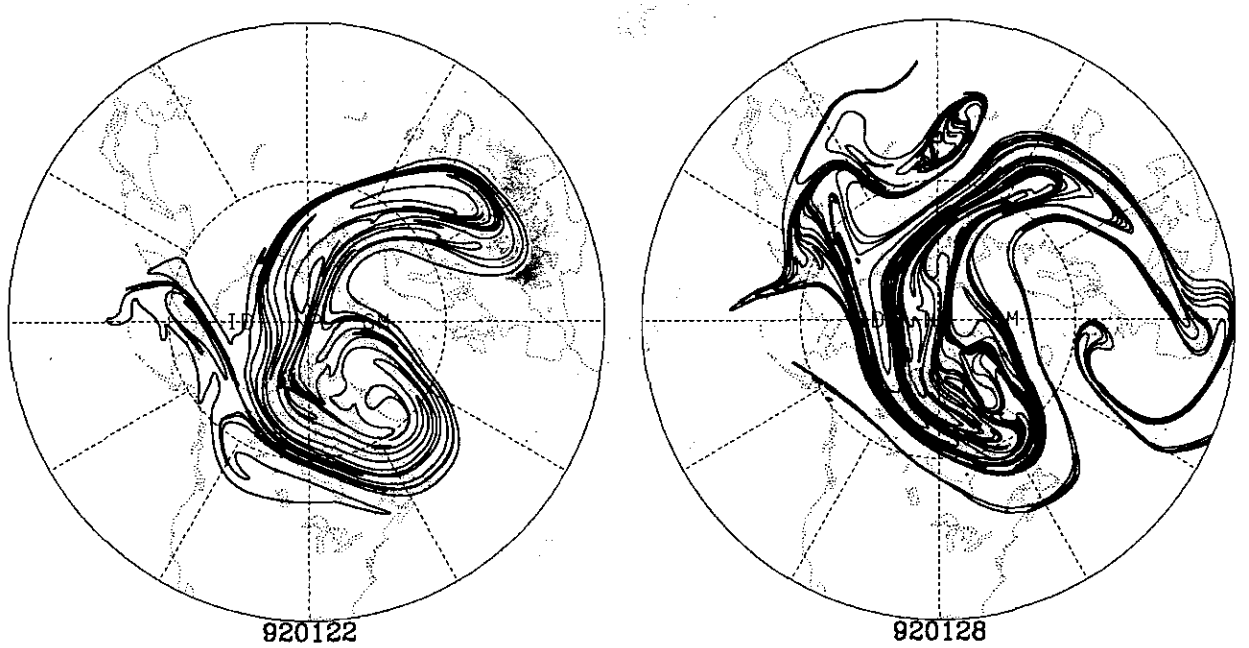

FIG. 10. Results of a CAS calculation from 1200 UTC 16 January 1992, using NMC analyzed winds on the 450 K isentropic surface to advect the contours. At the start of the calculation, the contours are put at the analyzed locations of the contours of Ertel PV on the 450 K surface; see Fig. 9a. Plot (a) shows the contours after 6 days, and (b) contours after 12 days, and should be compared with the analyzed location of these contours at that time, shown in Fig. 9.

calculation is continued, the particles become widely separated, it is difficult to form the shape of the contour, and many features are missed (e.g., the outbreak at 80°W on 28 January). The number of particles in the CAS calculation increases exponentially (there is approximately a tenfold increase in the number of particles during the 12-day calculation), and the rate of this increase (or more precisely, the increase of the length of the material contour) gives a measure of the rate of stirring. The rate of increase of material contours in CAS calculations using NMC data is presently under investigation.

6. Discussion

In this paper we have described a trajectory technique, CAS, for investigating the finescale structures in the material motion within a specified flow. CAS calculations can accurately produce finescale structures that are not explicitly present in the low-resolution input data (and cannot easily be reproduced using standard trajectory codes). Results from CAS calculations are relatively insensitive to the spatial resolution of the advecting wind field (primarily because the large-scale motions in the flow dominate the deformation field), and there are only small differences between calculations using wind fields with 1° resolution and those with 5° resolution. However, calculations from low-resolution winds can miss some of the details of the finescale structure, such as the roll-up of the tips of filaments, which are sensitive to the small-scale details of the flow. The results are, however, sensitive to the temporal resolution (errors such as spurious filamentary structures may develop if the advecting wind field is not stored often enough), and the necessary temporal resolution depends on the flow being analyzed. The more rapidly the material contours are evolving the higher the temporal resolution required for accurate CAS calculations.

A very simple measure of how rapidly a flow is evolving (and hence the required time interval for CAS calculations) is

$$\tau = U\Delta t/|\Delta u|_{\max},$$

where U is a characteristic flow speed (e.g., zonal velocity of jet) and $\Delta u_{\max}$ is the change in velocity (at a fixed point) in time interval Δt. In the CDS calculation in section 3 the zonal velocity of the jet U is of the order of 40 m s^{-1}, while the maximum change in velocity in a day Δu is of the order of 80 m s^{-1}, so $\tau \approx 12$ h. On the other hand, for the SKYHI data considered in section 4, $U \approx 30$ m s^{-1} and $\Delta u_{\max} \approx 20$ m s^{-1}, yielding $\tau \approx 36$ h. These values of τ are consistent with the time interval for accurate CAS calculations determined in sections 3 and 4, although accurate calculations can still be performed for slightly larger time intervals; for example, $\Delta T = 18$ h in section 3. For the NMC data in section 5, $\tau \approx 18$ h, suggesting that daily stratospheric anal-

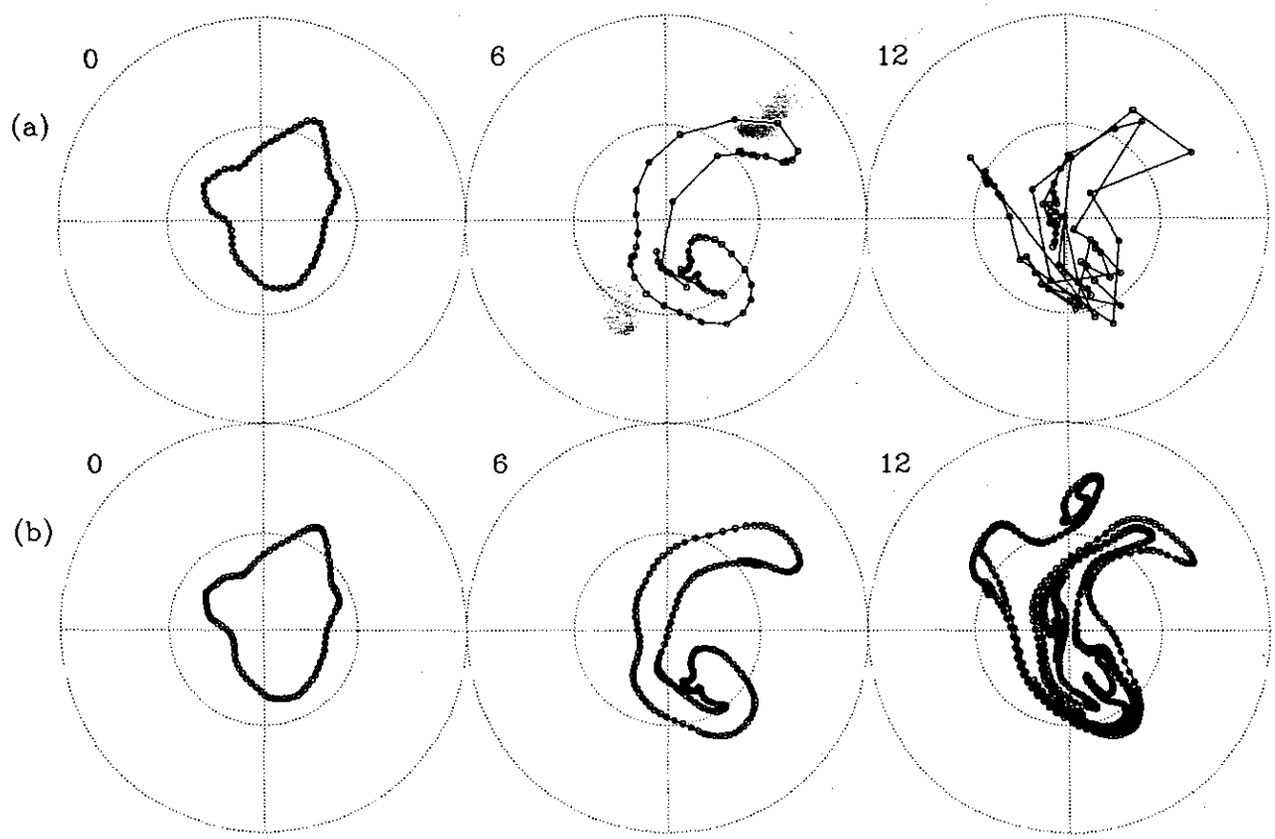

FIG. 11. Evolution of the 3.2×10^{-5} K m^2 s^{-1} kg^{-1} contour of Ertel PV for the period shown in Fig. 9, using (a) a standard trajectory code with 68 material particles and (b) the CAS code. Time (in days) is to the upper left of each plot; day 0 corresponds to 1200 UTC 16 January 1992. Circles represent position of material particles, and consecutive particles have been connected by straight lines. Plots are polar stereographic projections; latitudinal circles at 30° and 60° are marked, and 0° longitude is at the bottom of each plot.

yses will produce reasonably accurate CAS calculations.[1]

It has been shown that CAS calculations enable investigation of finescale structures in stratospheric tracer transport. The technique is currently being used (with NMC stratospheric analyses) to examine the generation of filamentary potential vorticity in the wintertime stratosphere and to investigate the isolation of material inside the polar vortex and the fate of material ejected from the polar vortex. It is also planned to use the technique to investigate tracer transport in the troposphere, although the accuracy of CAS computations of tropospheric flows has yet to be tested. The more active tropospheric flow may require a finer temporal resolution for accurate CAS calculations than is provided by twice-daily analyses, and there may also be doubts about the validity of the assumption of quasi-two-dimensional, adiabatic motion.

[1] Further calculations using data from the ECMWF forecast model, stored at 6-h intervals, confirm that accurate CAS calculations can be performed using daily analyses.

Acknowledgments. The authors thank David Dritschel for the original contour surgery code; Noboru Nakamura for providing the GFDL SKYHI data; Paul Newman for providing the NMC stratospheric analyses; and Roger Atkinson, Michael McIntyre, Lorenzo Polvani, and Mark Schoeberl for helpful discussions. We also thank anonymous reviewers for their helpful comments. This work was supported by the National Science Foundation through Grants ATM-9015367 and ATM-9245804, and by the NASA High Speed Research Program through Grant NAG-1-1360. The early development of this work was begun as a part of the second Arctic Airborne Stratosphere Experiment, participation in which was supported by the Alternative Fluorocarbon Acceptability Study through Contract CTR SP91-17.1. Some computations were performed on the Cray Y-MP at the Pittsburgh Supercomputing Center through Grant ATM920001P. The original CDS calculation was performed while DWW was at the Dept. of Applied Mathematics and Theoretical Physics, Cambridge, UK, with support through the Association of Commonwealth Universities, the U.S. Office of Naval Research, and NERC

through the U.K. Universities' Global Atmospheric Modeling Project.

REFERENCES

Anderson, J. G., W. H. Brune, and M. H. Proffitt, 1989: Ozone destruction by chlorine radicals within the Antarctic vortex: The spatial and temporal evolution of ClO-O_3 anticorrelation based on in situ ER-2 data. *J. Geophys. Res.*, **94**(D9), 11 465–11 480.

Dritschel, D. G., 1988: Contour surgery: A topological reconnection scheme for extended integrations using contour dynamics. *J. Comput. Phys.*, **77**, 240–266.

——, 1989: Contour dynamics and contour surgery: Numerical algorithms for extended, high-resolution modeling of vortex dynamics in two-dimensional, inviscid, incompressible flows. *Comput. Phys. Rep.*, **10**, 77–146.

Juckes, M. N., 1989: A shallow water model of the winter stratosphere. *J. Atmos. Sci.* **46**, 2934–2954.

Mahlman, J. D., and L. J. Umscheid, 1987: Comprehensive modeling of the middle atmosphere: The influence of horizontal resolution. *Transport Processes in the Middle Atmosphere,* G. Visconti and R. R. Garcia, Eds., D. Reidel, 251–266.

Murphy, D. M., A. F. Tuck, K. K. Kelly, K. R. Chan, M. Loewenstein, J. R. Podolske, M. R. Proffitt, and S. E. Strahan, 1989: Indicators of transport and vertical motion from correlations between in situ measurements in the airborne Antarctic ozone experiment. *J. Geophys. Res.*, **94**(D9), 11 669–11 685.

Norton, W. A., 1994: Breaking Rossby waves in a model stratosphere diagnosed by a vortex-following coordinate system and a technique for advecting material contours. *J. Atmos. Sci.*, **51**, 654–673.

Pierce, B. R., and T. D. A. Fairlie, 1993: Chaotic advection in the stratosphere: Implications for the dispersal of chemically perturbed air from the polar vortex. *J. Geophys. Res.*, **98**, 18 589–18 595.

Plumb, R. A., D. W. Waugh, R. J. Atkinson, M. R. Schoeberl, L. R. Lait, P. A. Newman, E. V. Browell, A. Simmons, M. Loewenstein, D. W. Toohey, and L. M. Avallone, 1994: Intrusions into the lower stratospheric arctic vortex during the winter of 1991/92. *J. Geophys. Res.*, in press.

Salby, M. L., R. R. Garcia, D. O'Sullivan, and P. Callaghan, 1990: The interaction of horizontal eddy transport and thermal drive in the stratosphere. *J. Atmos. Sci.*, **47**, 1647–1665.

Schoeberl, M. R., and J. T. Bacmeister, 1993: Mixing processes in the extra tropical stratosphere. *The Role of the Stratosphere in Global Change,* M. L. Chanin, Ed., Springer-Verlag, 135–152.

Tuck, A. F., T. Davies, S. J. Hovde, M. Noguer-Alba, D. W. Fahey, S. R. Kawa, K. K. Kelly, D. M. Murphy, M. R. Proffitt, J. J. Margitan, M. Loewenstein, J. R. Podolske, S. E. Strahan, and K. R. Chan, 1992: Polar stratospheric cloud processed air and potential vorticity in the Northern Hemisphere lower stratosphere at mid-latitudes during winter. *J. Geophys. Res.*, **97**(D8), 7883–7904.

Waugh, D. W., 1993: Contour surgery simulations of a forced polar vortex. *J. Atmos. Sci.*, **50**, 714–730.

——, R. A. Plumb, R. J. Atkinson, M. R. Schoeberl, L. R. Lait, P. A. Newman, M. Loewenstein, D. W. Toohey, L. M. Avallone, C. R. Webster, and R. D. May, 1994: Transport of material out of the stratospheric Arctic vortex by rossby wave breaking. *J. Geophys. Res.*, in press.